Journal of Materials Chemistry A

Accepted Manuscript

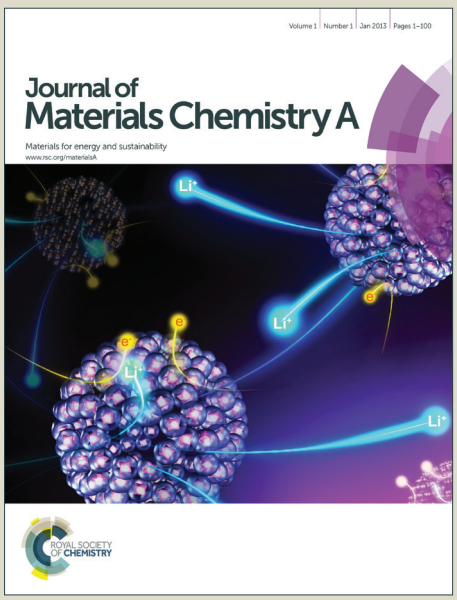

ROYAL SOCIETY OF CHEMISTRY

www.rsc.org/materialsA

Surfactant-free synthesis of reduced graphene oxide supported porous PtAu alloyed nanoflowers with improved catalytic activity

Pei Song, Li-Li He, Ai-Jun Wang, Li-Ping Mei, Shu-Xian Zhong, Jian-Rong Chen, Jiu-Ju Feng*

College of Chemistry and Life Science, College of Geography and Environmental Science, Zhejiang Normal University, Jinhua, 321004, China

**Corresponding author: jjfeng@zjnu.cn (JJF), Tel./Fax: +86 579 82282269.*

Abstract

A simple and facile one-pot wet-chemical co-reduction method was developed for synthesis of reduced graphene oxide supported porous PtAu alloyed nanoflowers (PtAu-nanoflowers/rGO). *p*-Aminopyridine was employed as a structure-directing agent and a stabilizing agent. No any seed, template, surfactant, or polymer was involved in the synthesis process. It was found that the reaction temperature and the dosage of *p*-aminopyridine were essential to the final product. Furthermore, the as-prepared nanocomposites showed improved catalytic activity for the reduction of 4-nitrophenol in contrast to monometallic Pt nanocrystals/rGO, Au nanocrystals/rGO, and commercial Pt/C (50 wt %).

Keywords: Reduced graphene oxide; Bimetallic nanoflowers; 4-Nitrophenol, Catalytic activity

1. Introduction

Bimetallic nanomaterials have attracted increasing attention in catalysis, electronics, and optics,[1-4] owing to their unique bifunctional mechanism and electronic effects between the two components.[5] For example, PtAu alloyed nanocrystals displayed improved catalytic performance and better stability toward a variety of reactions.[6] In another example, PtCo alloyed networks were synthesized for methanol oxidation reaction, which showed enhanced CO tolerance as compared to single Pt nanoparticles, owing to the modified electron structure of Pt by Co in PtCo alloy.[7]

More importantly, PtAu nanocrystals display improved catalytic properties in comparison with their respective monometallic counterparts.[8, 9] Thus, a variety of structures have been prepared.[10-14] Core-shell Au@Pt nanostructures were fabricated by seed-mediated overgrowth.[10] PtAu nanotubes were constructed by galvanic replacement, using Ag nanowires as the sacrificial template.[11] Hollow PtAu nanostructures were prepared by galvanic replacement between Co nanoparticles and Pt and Au precursors.[12] PtAu nanodendrites were obtained by electrodeposition.[13] And porous PtAu nanoparticles were formed by co-chemical reduction.[14]

Among the above nanostructures, three-dimensional porous nanostructures have drawn tremendous attention, which contribute to large specific surface area and provide more active sites available for the abundant atomic steps, edges, and corner atoms on their branches.[15-17] Moreover, the typical interconnected structures can effectively suppress the Ostwalding ripening effects, and consequently increase their durability.[18, 19]

Graphene serves as a promising carbon-based support to load bimetallic catalysts, owing to their good electrical conductivity, large specific surface area, and high mechanical strength.[20] The resulting nanocomposites combine the features of individual components, and have potential functions with enhanced performance.[21] As a result, a lot of graphene supported bimetallic catalysts were prepared, including PdAu/graphene,[22] PdNi/graphene,[23] PtAu/graphene,[24] and AuAg/graphene[25]. For example, PtPd/graphene were fabricated in our group, which exhibited excellent electrocatalytic properties for methanol and ethanol oxidation.[26] He and co-workers synthesized AuPd/graphene catalysts, which had a better performance for the reduction of 4-nitrophenol (4-NP).[27]

Conventionally, 4-aminophenol (4-AP) is usually produced by the reduction of 4-NP, which is a vital intermediate for fabrication of diverse analgesic and antipyretic drugs, anticorrosion lubricants, and hair drying agents.[28, 29] Conventionally, the way to produce 4-AP in the presence of iron-acid sometimes brings severe environmental problem.[30] Therefore, it is crucial to develop environmental benign and economical catalysts for preparation of 4-AP. Alternatively, an green and facile way is developed for introduction of nano-scaled catalysts to produce 4-AP, through directly catalyzing hydrogenation of 4-NP in the presence of sodium borohydride ($NaBH_4$).[31]

Herein, a simple and facile one-pot method was developed for synthesis of flower-like PtAu nanostructures anchored on reduced graphene oxide (PtAu-nanoflowers/rGO). The catalytic performance of the as-synthesized nanocomposites was investigated in some detail, using the reduction of 4-NP as a

model system.

2. Experimental section

2.1 Chemicals

Graphite powder (8000 meshes), chlorauric acid ($HAuCl_4$), chloroplatinic acid ($H_2PtCl_6 \cdot 6H_2O$), *p*-aminopyridine, ascorbic acid (AA), sodium borohydride ($NaBH_4$), commercial Pt/C (50 wt %), and 4-nitrophenol (4-NP) were purchased from Aladdin Chemistry Co. Ltd (Shanghai, China). All the other chemicals were of analytical grade and used without further purification. All the aqueous solutions were prepared with twice-distilled water in the whole experiments.

2.2 Synthesis of catalysts

Graphene oxide nanosheets (GO) were firstly prepared from natural graphite powder via acid-oxidation according to a modified Hummers' method.[32] To obtain the exfoliated GO, the resultant GO suspension was further ultrasonicated for 30 min.

For typical preparation of porous PtAu-nanoflowers/rGO, the aqueous solution of GO suspension was ultrasonicated for 30 min to get a homogeneous dispersion. Then, 2 mL GO suspension (1 mg mL^{-1}), 100 μL $HAuCl_4$ (24.3 mM), and 63 μL H_2PtCl_6 (38.62 mM) were successively put into 7 mL *p*-aminopyridine solution (14.3 mM) under stirring. Afterward, 1 mL AA (0.1 M) was slowly dropped into the above mixed solution. The mixture was heated in a water-bath at 80 °C for 30 min with gentle agitation. The final products were collected by centrifugation, washed with

water and ethanol, and then dried in vacuum for further characterization.

For comparison, monometallic Pt and Au nanocrystals (NCs) supported on rGO (denoted as Pt NCs/rGO and Au NCs/rGO) were prepared in a similar way, using H_2PtCl_6 and $HAuCl_4$ as the precursors, while other conditions were kept the same.

2.3 Characterization

Transmission electron microscopy (TEM), high-resolution TEM (HRTEM), high-angle annular dark-field scanning transmission electron microscopy (HAADF-STEM), elemental mapping, and energy-dispersive X-ray spectroscopy (EDS) were performed on a JEM-2100F microscope operated at an acceleration voltage of 200 kV. X-ray diffraction (XRD) spectra were measured on a Rigaku Dmax-2000 diffractometer using Cu Kα radiation source (λ = 0.15418 nm). X-ray photoelectron spectroscopy (XPS) measurements were conducted on a K-Alpha XPS (ThermoFisher, E. Grinstead, UK) with an Al Kα X-ray radiation (1486.6 eV photons) for excitation. Raman spectra were acquired at a Renishaw Raman system model 1000 spectrometer equipped with a CCD detector, using a He/Ne laser at a wavelength of 633 nm. Thermogravimetric analysis (TGA) was carried out in air on a NETZSCH STA 449C thermogravimetric analyzer. The samples were heated from 25 to 900 °C with the heating rate of 10 °C min^{-1}.

2.4 General procedure for 4-nitrophenol reduction

The aqueous solutions of 4-NP (0.7 mM) and $NaBH_4$ (0.5 M) were freshly

prepared. Briefly, 500 μL of the 4-NP suspension and 1 mL of $NaBH_4$ solution were mixed with 1 mL of water in a quartz cuvette, leading to the formation of a yellow mixed solution. After the injection of PtAu-nanoflowers/rGO suspension (1 mg mL^{-1}) into the above cuvette, the associated UV-vis spectra were quickly recorded in a scanning range of 250 ~ 550 nm. The absorption peak intensity at 400 nm was monitored by UV-vis spectroscopy as a function of time. When the reaction was finished, the solution color changed from yellowish green to colorless. Following the similar procedures, commercial Pt/C (50 wt %), Pt NCs/rGO, and Au NCs/rGO were also used as heterogeneous catalysts for 4-NP reduction in control experiments.

Next, the cyclic catalytic reduction reaction of 4-NP was performed according to the previous work.[33] In the recycling test, the aqueous solutions of 4-NP (7 mM) and $NaBH_4$ (0.5 M) were freshly prepared. 50 μL of 4-NP solution and 1 mL of $NaBH_4$ solution were mixed with 1.2 mL of water in a quartz cuvette. Then, 50 μL of the as-prepared PtAu-nanoflowers/rGO suspension (1 mg mL^{-1}) was injected into the cuvette. The intensity of the absorption peak at 400 nm was monitored by UV-vis spectroscopy as a function of time. When the reduction cycle was finished, another 50 μL of 4-NP suspension were added to examine for recyclability.

3. Results and discussion

3.1. Characterization of PtAu-nanoflowers/rGO

Low-resolution TEM image (Fig. 1A-B) shows that the final products contain many flower-like nanocrystals with the average diameter of 49.85 nm (inset in Fig.

1A), which are uniformly dispersed on rGO (marked by the red arrows). The flower-like porous nanostructures are further illustrated by high-resolution TEM (HRTEM) image (Fig. 1C), which are composed of numerous primary grains with the average diameter of 4.2 nm. Furthermore, HRTEM images in the marked sections show the clear lattice fringes with the interplanar spacing distance of 0.235 nm. This value is smaller than that of the (111) crystal planes of the face-centered cubic (fcc) Au (0.236 nm, JCPDS-04-0784), but larger than that of the fcc Pt (0.227 nm, JCPDS-46-0802), indicating the formation of the fcc PtAu alloy. For comparison, TEM images of monometallic Au NCs/rGO and Pt NCs/rGO are also provided in Fig. S1 (Electronic supplementary information, ESI). Some wire-like Au NCs (Fig. S1A) and tiny Pt nanoparticles (Fig. S1B) are observed on rGO, respectively.

The EDS line scanning profiles (Fig. 2A) and elemental mapping patterns (Fig. 2B) demonstrate the homogeneous distribution of Pt and Au across a whole nanoparticle, manifesting the alloyed feature of PtAu nanoparticles. Furthermore, EDS analysis confirms the coexistence of Pt and Au in the present synthesis. And the atomic ratio of Pt to Au is 25.69:74.30 (Fig. S2, ESI).

Fig. 3 shows the XRD patterns of PtAu-nanoflowers/rGO (curve a), GO (curve b), bulk Pt (JCPDS-46-0802), and Au (JCPDS-04-0784). There are four representative diffraction peaks at 38.89°, 45.24°, 65.64°, and 79.13° for PtAu-nanoflowers/rGO, which are well indexed to the (111), (200), (220), and (311) planes of the fcc PtAu alloy.[24, 34]Notably, these peaks are coincidently located between those of bulk Pt and Au, verifying the formation of PtAu alloy. Besides, according to the Scherrer's

equation,[14] the average crystallize size of PtAu grains in PtAu-nanoflowers is about 4.5 nm, which is calculated from the (111) diffraction peak, as supported by the HRTEM observation. In addition, a broad diffraction peak at 22.6° is found for PtAu-nanoflowers/rGO, which is unlike blank GO with a sharp peak centered at 11.0° corresponding to the (002) planes of GO, indicating the efficient reduction of GO to rGO.[35]

Raman is a conventional tool to monitor the structural change of graphene-based materials. Fig. 4A shows the Raman spectra of PtAu-nanoflowers/rGO (curve a) and GO (curve b). In each case, there are two distinguished characteristic peaks at 1342 and 1596 cm^{-1}, which are indexed to the *D* band correlated with the order/disorder of graphite structure and *G* band associated with the graphitic stacking structure.[26, 36] And the intensity ratio of *D* to *G* bands (I_D/I_G) indicates the degree of disorder and the average size of the in-plane sp^2 domains.[26, 37] The I_D/I_G of PtAu-nanoflowers/rGO is estimated to be about 1.57, which is larger than that of GO (0.82), reflecting the formation of partially ordered crystal structures and decreased size of in-plane sp^2 domains during the reduction of GO.[38]

The metal loading of PtAu-nanoflowers/rGO was obtained by TGA analysis (Fig. 4B, curve a). The weight loss below 100 °C, and in the range of 150~500 °C and 600~700 °C are attributed to water evaporation, pyrolysis of oxygenated functional groups, and combustion of carbon skeleton of rGO,[39] respectively. The steady weight loss between 150 and 500 °C for PtAu-nanoflowers/rGO is much different from GO with a sharp loss at around 200 °C (curve b), indicating the decrease of oxygenated

functional groups in rGO.[14] Additionally, the mass loading of PtAu nanoparticles is evaluated to be 28.99 % for PtAu-nanoflowers/rGO.

The surface oxidation states and compositions of PtAu-nanoflowers/rGO were investigated by XPS measurements (Fig. 5). As displayed in the survey XPS spectrum, the distinct peaks located at 73, 83, 284, and 531 eV are well assigned to Pt, Au, C, and O elements, respectively.

The Pt XPS spectrum can be divided into two pairs of peaks (Fig. 5B). The stronger peaks located at 69.98 eV (Pt $4f_{7/2}$) and 73.33 eV (Pt $4f_{5/2}$) are assigned to Pt^0, while the weaker ones detected at 71.89 eV (Pt $4f_{7/2}$) and 75.82 eV (Pt $4f_{5/2}$) correspond to Pt^{2+} in PtO or $Pt(OH)_2$.[40, 41] However, the Au 4f XPS spectra can only be divided into one pair of the peaks at 86.48 and 82.83 eV (Fig. 5C), suggesting that the Au precursors are completely reduced to metallic Au.[42] In addition, the peak of C 1s is located at 284.1 eV, which is fitted into three peaks at 283.73, 285.28, and 287.43 eV, corresponding to C−C (sp^2), C−O, and C=O groups,[43, 44] respectively. The oxygenated functional groups remarkably decrease for PtAu-nanoflowers/rGO, compared with those of GO (Fig. S3, ESI), suggesting the efficient reduction of GO to rGO.

3.2. Formation mechanism

To further investigate the formation mechanism of PtAu-nanoflowers/rGO, a series of control experiments were conducted. Firstly, temperature-dependent experiments were performed (Fig. 6). At the lower temperature of 40 °C, several

spherical nanoparticles were formed, accompanied with the emergence of sparse nanowires (Fig. 6A). With the increase of the temperature to 60 °C, the nanowires are shortened and further assembled to spherical nanoparticles (Fig. 6B), since newly generated primary nanocrystals are unstable and agglomerated together to reduce the overall surface energy.[45] And the best ones are obtained when the temperature achieves 80 °C (Fig. 1B), revealing that this synthesis is mainly controlled by thermodynamic model.[46] Alternatively, the freshly produced nanocrystals are seriously aggregated together, causing the formation of large irregular spherical agglomerates by using higher temperature of 100 °C (Fig. 6C).

It is worth noting that the absence of *p*-aminopyridine yields heavily aggregated spherical nanoparticles (Fig. 7A). PtAu nanoflowers with poor quality are produced in the presence of less *p*-aminopyridine (2.5 mM, Fig. 7B), while PtAu nanoflowers are disappeared by introducing excess *p*-aminopyridine (25 mM, Fig. 7C). The existence of *p*-aminopyridine may prevent newly formed nanocrystals from further aggregation and improve the shape-controlled synthesis, leading to the formation of PtAu nanoflowers with high quality. It clearly demonstrates that *p*-aminopyridine acts as an essential structure-directing agent and a stabilizing agent in the synthesis of PtAu-nanoflowers.

These results indicate that the formation mechanism of PtAu-nanoflowers is based on the rapid nucleation and self-assembly growth.[47, 48] After the addition of AA, Pt and Au atoms are generated during the initial stage, which rapidly nucleate when the concentrations of Pt and Au atoms have reached hyper-saturated states. Moreover,

the as-formed nuclei spontaneously aggregate together, resulting in the formation of spherical particles to minimize their surface energy. *p*-Aminopyridine is employed as a stabilizing agent and a structure-directing agent, which is selectively adsorbed onto the surfaces of the spherical particles, inducing smaller particles to further grow up and self-assemble, leading to the formation of uniform PtAu-nanoflowers on the rGO.

By replacing *p*-aminopyridine with poly(diallyldimethylammoniumchloride) (PDDA), graphene decorated with PtAu alloy nanoparticles was prepared by a two-step strategy in the control experiments.[24] In their work, PtAu alloy nanoparticles was firstly prepared, followed by mixing with the pre-prepared GO. Obviously, the as-developed one-pot wet-chemical co-reduction method for synthesis of PtAu-nanoflowers/rGO is simple and facile, in which there was no any seed, template, surfactant, or polymer involved. Furthermore, the as-obtained PtAu alloyed nanoflowers have large specific surface area and provide more active sites available. Additionally, the preparation time is greatly decreased from 3 h to 30 min as compared to Zhang's work.[24]

3.3. Catalytic performance of PtAu-nanoflowers/rGO

In general, the reduction of 4-NP to 4-AP with $NaBH_4$ is usually employed as a model reaction to determine the catalytic performance of catalysts.[49-51] Fig. 8 shows time-dependent UV-vis absorption spectra in the presence of PtAu-nanoflowers/rGO. After the successive addition of PtAu-nanoflowers/rGO, the absorption peak located at 400 nm gradually decreases, which is come from 4-NP.[52, 53] Besides, another peak

appears at 300 nm, corresponding to 4-AP. Therefore, the reaction rate can be easily assessed by tracking the respective peak intensities. Moreover, the solution color is changed from yellowish green to colorless. Specifically, 4-NP can be completely reduced to 4-AP within 6 min, as reflected by the disappearance of the peak of 4-NP in the presence of 0.05 mg PtAu-nanoflowers/rGO. Moreover, the reaction rate drops down by reducing the dosage of the catalyst. Schematic illustration of 4-NP reduction on PtAu-nanoflowers/rGO was shown in Fig. 9.

For comparison, the catalytic performance of commercial Pt/C (50 wt %), home-made Pt NCs/rGO, and Au NCs/rGO were investigated under the identical conditions. Fig. 10 displays the time-dependent UV-vis absorption spectra for the reduction of 4-NP by PtAu-nanoflowers/rGO (Fig. 10A), using Pt/C (Fig. 10B), Au NCs/rGO (Fig. 10C), and Pt NCs/rGO (Fig. 10D) as referenced materials. The peak emerges at 400 nm and disappears completely within 6 min for PtAu-nanoflowers/rGO. The reaction time is shorter than those of commercial Pt/C (12 min), Au NCs/rGO (12 min), and Pt NCs/rGO (14 min), showing the enhanced catalytic activity of PtAu-nanoflowers/rGO.

Moreover, pseudo-first-order can be used to calculate the reaction rate constant for 4-NP reduction because the concentration of $NaBH_4$ is significantly higher than that of 4-NP.[52, 54] The apparent rate constant (k_{app}) was assumed to be proportional to the surface (S) of the metal nanoparticles normalized to the unit volume of the system, then the kinetic constant (k_{app}) can be defined: $-dC_t/d_t = k_{app}C_t = k_1SC_t$, where C_t is the concentration of 4-NP at time t, and k_1 was the rate constant normalized to S.[55]

As illustrated in Fig. 10E, the k_{app} is obtained from the slope of the plot ($\ln(A_t/A_0)$ *vs*. time), where A_t and A_0 are the absorbance of 4-NP at time t and initial time, respectively. Table S1 (ESI) lists the k_{app} values of PtAu-nanoflowers/rGO, Pt/C, Pt NCs/rGO, and Au NCs/rGO for the catalytic reduction of 4-NP. It is found that 4-NP reduction reaction follows the pseudo-first-order kinetic model. Obviously, the k_{app} is calculated to be 12.4×10^{-3} s^{-1} for PtAu-nanoflowers/rGO, which is higher than those of Pt/C (7.08×10^{-3} s^{-1}), Pt NCs/rGO (4.96×10^{-3} s^{-1}), and Au NCs/rGO (6.18×10^{-3} s^{-1}), respectively.

In order to compare our results with the previous reports, the normalized rate constant (k_{nor}) was provided, which were obtained by normalizing the k_{app} values with respect to the amount of the catalysts (m), *i.e.*, $k_{nor} = k_{app}/m$.[56] Herein, metallic Pt and Au loading was measured to be 28.99 wt % in PtAu-nanoflowers/rGO according to TGA analysis, owing to the presence of rGO (Fig. 4B). The k_{nor} value of PtAu-nanoflowers/rGO is about 826.7 s^{-1} g^{-1} (as shown in Table S1, ESI), which is larger than Pt/C (283.2 s^{-1} g^{-1}), Pt NCs/rGO (99.2 s^{-1} g^{-1}), and Au NCs/rGO (123.6 s^{-1} g^{-1}). Moreover, this value is also larger than those of Ag@Au (53.6 s^{-1} g^{-1}),[57] AuPd nanocrystals (74 s^{-1} g^{-1}),[58] and PtAu nanocubes (33.3 s^{-1} g^{-1}).[59]

Recycling test was performed to explore the stability of the as-prepared PtAu-nanoflowers/rGO in this work (Fig. 10F and Fig. S4, ESI). As shown in Fig. 10F, within 10 cycles, the response time is almost remain constant in comparison with their initial values, indicating high stability of PtAu-nanoflowers/rGO toward 4-NP reduction. This assumption is strongly supported by the TEM image after ten

successive recycling reduction of 4-NP (Fig. S5, ESI). The morphology of PtAu-nanoflowers/rGO almost retains and nearly no agglomeration observed after the recyclability test.

The improved catalytic activity and stability of PtAu-nanoflowers/rGO is ascribed to the following reasons: (1) Synergistic catalytic effects of Pt and Au in bimetallic alloyed PtAu-nanoflowers play an important role. (2) The specific porous PtAu-nanoflowers structure provides more active sites available for 4-NP reduction. (3) The existence of rGO stabilizes the catalyst, prevents PtAu-nanoflowers form aggregation, and enlarges the active surface area of PtAu-nanoflowers. Additionally, its high electric conductivity facilitates the electron transport in catalytic reaction process.[20, 57]

4. Conclusions

In summary, bimetallic porous PtAu-nanoflowers/rGO was synthesized by a simple, facile, and one-pot wet-chemical co-reduction method, using *p*-aminopyridine as a stabilizing agent and a structure-directing agent. No seed, template, surfactant, or polymer was employed. The as-prepared nanocomposites showed improved catalytic performances for 4-NP reduction as compared to the other catalysts. This method can be explored for preparation of others bimetallic alloys with high catalytic activity, using specific organic compounds as a stabilizing agent and a structure-directing agent.

Acknowledgments

This work was financially supported by the National Natural Science Foundation of China (21475118, 21175118, 21275130 and 21275131) and Colleges in Zhejiang province to the young academic leaders of academic climbing project (pd2013055).

References

1. W. Hong, J. Wang and E. Wang, *ACS Appl. Mat. Interfaces*, 2014, **6**, 9481-9487.
2. R. Su, R. Tiruvalam, Q. He, N. Dimitratos, L. Kesavan, C. Hammond, J. A. Lopez-Sanchez, R. Bechstein, C. J. Kiely, G. J. Hutchings and F. Besenbacher, *ACS Nano*, 2012, **6**, 6284-6292.
3. J. Zeng, C. Zhu, J. Tao, M. Jin, H. Zhang, Z.-Y. Li, Y. Zhu and Y. Xia, *Angew. Chem. Int. Ed.*, 2012, **51**, 2354-2358.
4. H. Wang, Z. Sun, Y. Yang and D. Su, *Nanoscale*, 2013, **5**, 139-142.
5. A. K. Singh and Q. Xu, *ChemCatChem*, 2013, **5**, 652-676.
6. G.-R. Zhang, D. Zhao, Y.-Y. Feng, B. Zhang, D. S. Su, G. Liu and B.-Q. Xu, *ACS Nano*, 2012, **6**, 2226-2236.
7. J. Xu, X. Liu, Y. Chen, Y. Zhou, T. Lu and Y. Tang, *J. Mater. Chem.*, 2012, **22**, 23659-23667.
8. A. L. Allred, *J. Inorg. Nucl. Chem.*, 1961, **17**, 215-221.
9. Y. Bing, H. Liu, L. Zhang, D. Ghosh and J. Zhang, *Chem. Soc. Rev.*, 2010, **39**, 2184-2202.
10. Y. Kim, J. W. Hong, Y. W. Lee, M. Kim, D. Kim, W. S. Yun and S. W. Han,

Angew. Chem. Int. Ed., 2010, **49**, 10197-10201.

11. Y. Kim, H. J. Kim, Y. S. Kim, S. M. Choi, M. H. Seo and W. B. Kim, *J. Phys. Chem. C*, 2012, **116**, 18093-18100.
12. H.-P. Liang, Y.-G. Guo, H.-M. Zhang, J.-S. Hu, L.-J. Wan and C.-L. Bai, *Chem. Commun.*, 2004, 1496-1497.
13. Y. Hu, H. Zhang, P. Wu, H. Zhang, B. Zhou and C. Cai, *Phys. Chem. Chem. Phys.*, 2011, **13**, 4083-4094.
14. J.-N. Zheng, S.-S. Li, X. Ma, F.-Y. Chen, A.-J. Wang, J.-R. Chen and J.-J. Feng, *J. Mater. Chem. A*, 2014, **2**, 8386-8395.
15. B. Lim and Y. Xia, *Angew. Chem. Int. Ed.*, 2011, **50**, 76-85.
16. F. Wang, C. Li, L.-D. Sun, C.-H. Xu, J. Wang, J. C. Yu and C.-H. Yan, *Angew. Chem. Int. Ed.*, 2012, **51**, 4872-4876.
17. L. Wang and Y. Yamauchi, *J. Am. Chem. Soc.*, 2010, **132**, 13636-13638.
18. M. Gong, G. Fu, Y. Chen, Y. Tang and T. Lu, *ACS Appl. Mat. Interfaces*, 2014, **6**, 7301-7308.
19. W. Wang, D. Wang, X. Liu, Q. Peng and Y. Li, *Chem. Commun.*, 2013, **49**, 2903-2905.
20. X. Huang, X. Qi, F. Boey and H. Zhang, *Chem. Soc. Rev.*, 2012, **41**, 666-686.
21. C. Tan, X. Huang and H. Zhang, *Mater. Today*, 2013, **16**, 29-36.
22. J.-N. Zheng, S.-S. Li, X. Ma, F.-Y. Chen, A.-J. Wang, J.-R. Chen and J.-J. Feng, *J. Power Sources*, 2014, **262**, 270-278.
23. Y. She, Z. Lu, W. Fan, S. Jewell and M. K. H. Leung, *J. Mater. Chem. A*, 2014, **2**,

3894-3898.

24. S. Zhang, Y. Shao, H.-G. Liao, J. Liu, I. A. Aksay, G. Yin and Y. Lin, *Chem. Mater.*, 2011, **23**, 1079-1081.

25. T. Wu, L. Zhang, J. Gao, Y. Liu, C. Gao and J. Yan, *J. Mater. Chem. A*, 2013, **1**, 7384-7390.

26. S.-S. Li, J.-N. Zheng, X. Ma, Y.-Y. Hu, A.-J. Wang, J.-R. Chen and J.-J. Feng, *Nanoscale*, 2014, **6**, 5708-5713.

27. Y. He, N. Zhang, L. Zhang, Q. Gong, M. Yi, W. Wang, H. Qiu and J. Gao, *Mater. Res. Bull.*, 2014, **51**, 397-401.

28. J. Li, C.-Y. Liu and Y. Liu, *J. Mater. Chem.*, 2012, **22**, 8426-8430.

29. P. Zhang, C. Shao, Z. Zhang, M. Zhang, J. Mu, Z. Guo and Y. Liu, *Nanoscale*, 2011, **3**, 3357-3363.

30. H. Lu, H. Yin, Y. Liu, T. Jiang and L. Yu, *Catal. Commun.*, 2008, **10**, 313-316.

31. T. R. Mandlimath and B. Gopal, *J. Mol. Catal. A: Chem.*, 2011, **350**, 9-15.

32. N. I. Kovtyukhova, P. J. Ollivier, B. R. Martin, T. E. Mallouk, S. A. Chizhik, E. V. Buzaneva and A. D. Gorchinskiy, *Chem. Mater.*, 1999, **11**, 771-778.

33. Y. Liu, Z. Fang, L. Kuai and B. Geng, *Nanoscale*, 2014, **6**, 9791-9797.

34. J. Xu, T. Zhao, Z. Liang and L. Zhu, *Chem. Mater.*, 2008, **20**, 1688-1690.

35. Y. Li, W. Gao, L. Ci, C. Wang and P. M. Ajayan, *Carbon*, 2010, **48**, 1124-1130.

36. Y. Kim, Y. Noh, E. J. Lim, S. Lee, S. M. Choi and W. B. Kim, *J. Mater. Chem. A*, 2014, **2**, 6976-6986.

37. M. Liu, Y. Lu and W. Chen, *Adv. Funct. Mater.*, 2013, **23**, 1289-1296.

38. S.-S. Li, J.-J. Lv, L.-N. Teng, A.-J. Wang, J.-R. Chen and J.-J. Feng, *ACS Appl. Mat. Interfaces*, 2014, **6**, 10549-10555.

39. S. Sharma, A. Ganguly, P. Papakonstantinou, X. Miao, M. Li, J. L. Hutchison, M. Delichatsios and S. Ukleja, *J. Phys. Chem. C*, 2010, **114**, 19459-19466.

40. J.-J. Lv, J.-N. Zheng, Y.-Y. Wang, A.-J. Wang, L.-L. Chen and J.-J. Feng, *J. Power Sources*, 2014, **265**, 231-238.

41. J. Yang, W. Zhou, C. H. Cheng, J. Y. Lee and Z. Liu, *ACS Appl. Mat. Interfaces*, 2009, **2**, 119-126.

42. F. Li, Y. Guo, R. Li, F. Wu, Y. Liu, X. Sun, C. Li, W. Wang and J. Gao, *J. Mater. Chem. A*, 2013, **1**, 6579-6587.

43. L. Gao, W. Yue, S. Tao and L. Fan, *Langmuir*, 2012, **29**, 957-964.

44. M. S. Arif Sher Shah, K. Zhang, A. R. Park, K. S. Kim, N.-G. Park, J. H. Park and P. J. Yoo, *Nanoscale*, 2013, **5**, 5093-5101.

45. J. Xie, Q. Zhang, J. Y. Lee and D. I. C. Wang, *ACS Nano*, 2008, **2**, 2473-2480.

46. M.-R. Gao, S.-R. Zhang, Y.-F. Xu, Y.-R. Zheng, J. Jiang and S.-H. Yu, *Adv. Funct. Mater.*, 2014, **24**, 916-924.

47. S. Wang, X. Wang and S. P. Jiang, *Phys. Chem. Chem. Phys.*, 2011, **13**, 6883-6891.

48. H. Ataee-Esfahani, L. Wang, Y. Nemoto and Y. Yamauchi, *Chem. Mater.*, 2010, **22**, 6310-6318.

49. X. Zhang and Z. Su, *Adv. Mater.*, 2012, **24**, 4574-4577.

50. Y. Sun and C. Lei, *Angew. Chem. Int. Ed.*, 2009, **48**, 6824-6827.

51. X. Huang, Y. Li, H. Zhou, X. Zhong, X. Duan and Y. Huang, *Chem. Eur. J.*, 2012, **18**, 9505-9510.

52. L. Chen, L. Kuai, X. Yu, W. Li and B. Geng, *Chem. Eur. J.*, 2013, **19**, 11753-11758.

53. Y. Imura, K. Tsujimoto, C. Morita and T. Kawai, *Langmuir*, 2014, **30**, 5026-5030.

54. J. Liu, Q. Wu, F. Huang, H. Zhang, S. Xu, W. Huang and Z. Li, *RSC Advances*, 2013, **3**, 14312-14321.

55. Z. Zhang, C. Shao, P. Zou, P. Zhang, M. Zhang, J. Mu, Z. Guo, X. Li, C. Wang and Y. Liu, *Chem. Commun.*, 2011, **47**, 3906-3908.

56. W. Ye, Y. Chen, F. Zhou, C. Wang and Y. Li, *J. Mater. Chem.*, 2012, **22**, 18327-18334.

57. C.-H. Liu, X.-Q. Chen, Y.-F. Hu, T.-K. Sham, Q.-J. Sun, J.-B. Chang, X. Gao, X.-H. Sun and S.-D. Wang, *ACS Appl. Mat. Interfaces*, 2013, **5**, 5072-5079.

58. J. Zhang, C. Hou, H. Huang, L. Zhang, Z. Jiang, G. Chen, Y. Jia, Q. Kuang, Z. Xie and L. Zheng, *Small*, 2013, **9**, 538-544.

59. G. Fu, L. Ding, Y. Chen, J. Lin, Y. Tang and T. Lu, *CrystEngComm*, 2014, **16**, 1606-1610.

Captions

Fig. 1 TEM (A-B) and HRTEM (C-D) images of PtAu-nanoflowers/rGO. Inset shows the corresponding histogram of the particle-size distribution.

Fig. 2 Cross-sectional compositional line profiles (A) and HAADF-STEM-EDS elemental mapping images (B-D) taken from a single PtAu-nanoflowers.

Fig. 3 XRD pattern of PtAu-nanoflowers/rGO.

Fig. 4 Raman spectra (A) and TGA thermograms (B) of PtAu-nanoflowers/rGO.

Fig. 5 Survey (A), high-resolution Pt 4f (B), Au 4f (C), and C 2p (D) XPS spectra of PtAu-nanoflowers/rGO.

Fig. 6 TEM images of the products collected at different temperature: 40 °C (A), 60 °C (B), and 100 °C (C).

Fig. 7 TEM images of the products obtained in the absence (A) and presence of 2.5 mM (B) and 25 mM *p*-aminopyridine (C).

Fig. 8 Time-dependent UV-vis spectral changes in 4-nitropenol catalyzed by different

dosage of PtAu-nanoflowers/rGO: (A) 0.05 mg; (B) 0.035 mg; (C) 0.02 mg, and 0.01 mg (D).

Fig. 9 Schematic illustration of 4-NP reduction on PtAu-nanoflowers/rGO.

Fig. 10 Time-dependent UV-vis spectral changes in 4-NP catalyzed by 0.05 mg of PtAu-nanoflowers/rGO (A), Pt/C (B), Au NCs/rGO (C), and Pt NCs/rGO (D). (E) Plots of $\ln(A_t/A_0)$ *vs*. reaction time for 4-nitropenol reduction catalyzed by PtAu-nanoflowers/rGO, Au NCs/rGO, and Pt NCs/rGO. (F) Cycle time of ten successive reduction reactions with 0.05 mg PtAu-nanoflowers/rGO.

Figures

Fig. 1

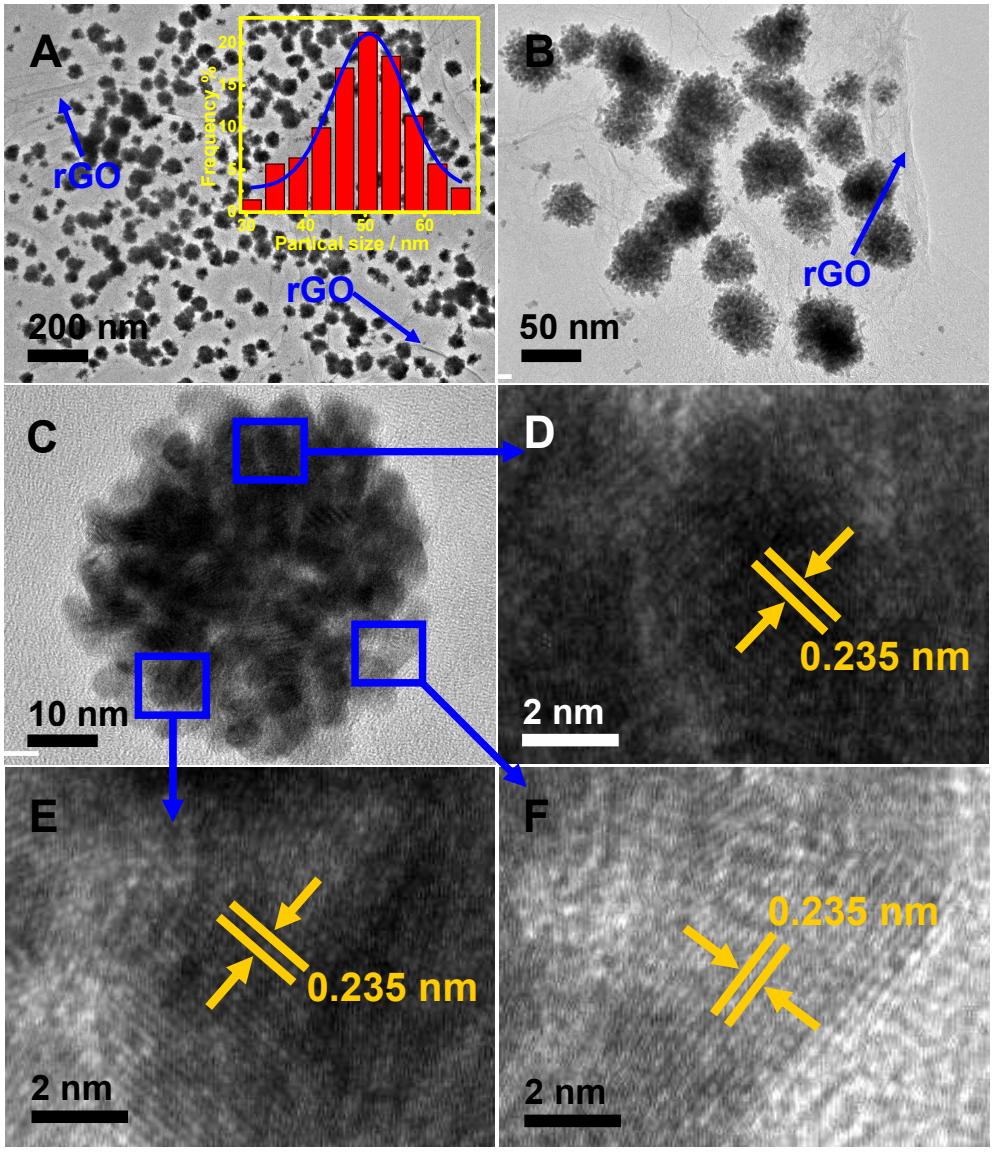

Fig. 2

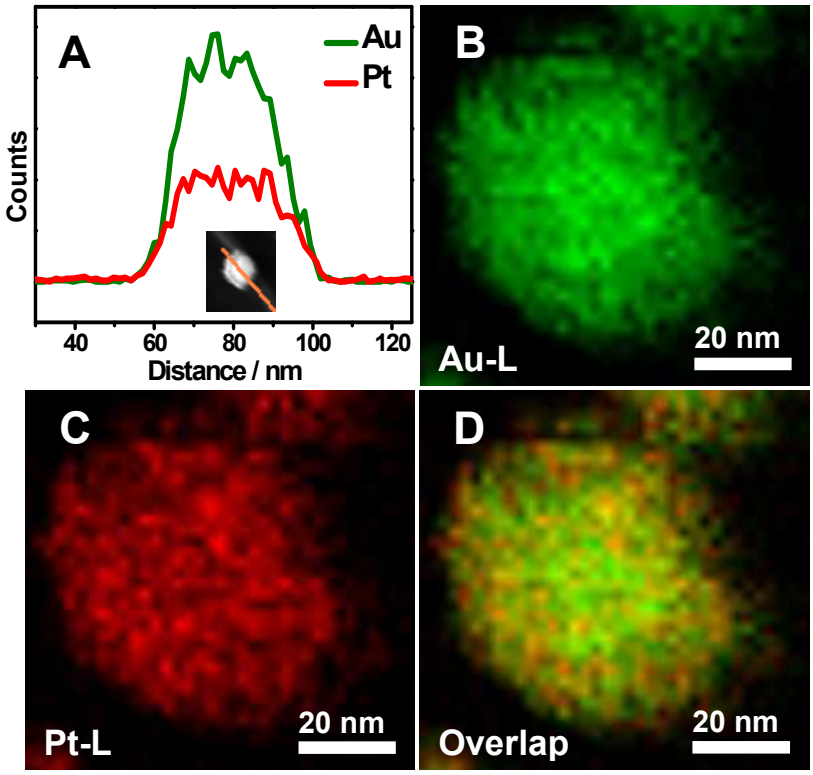

Fig. 3

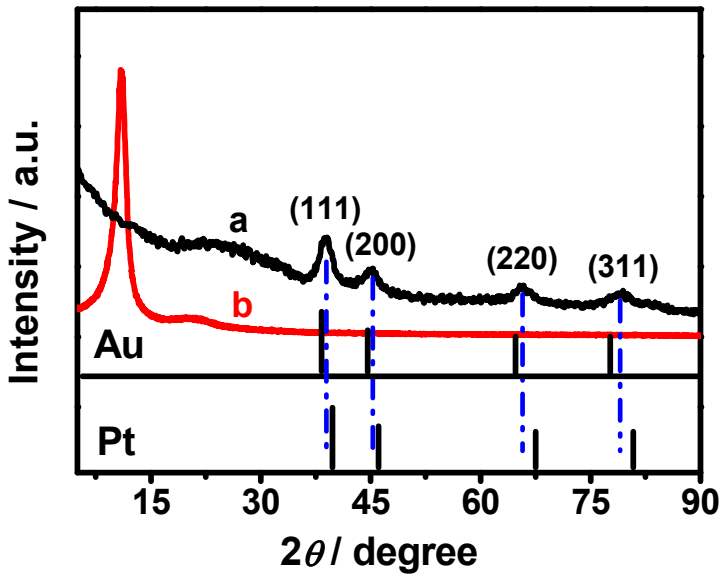

Fig. 4

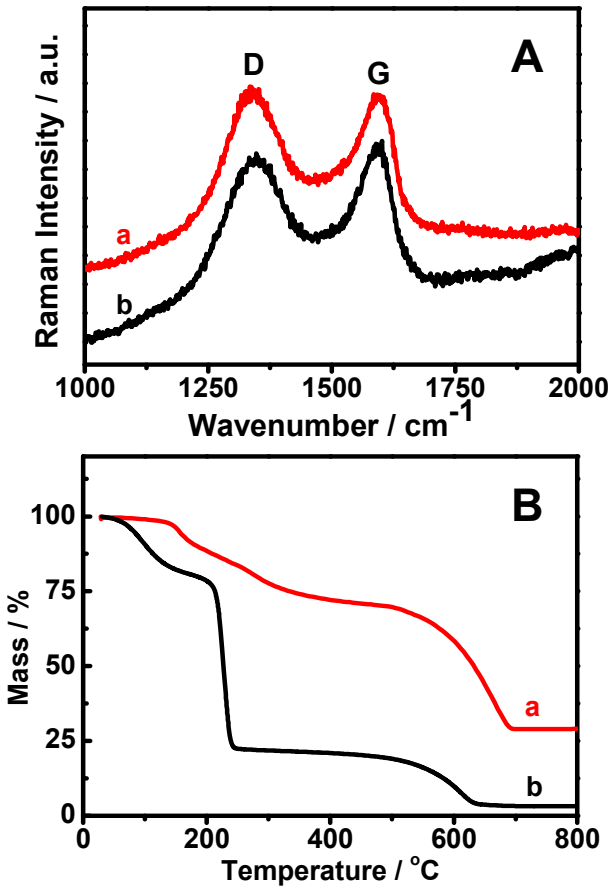

Fig. 5

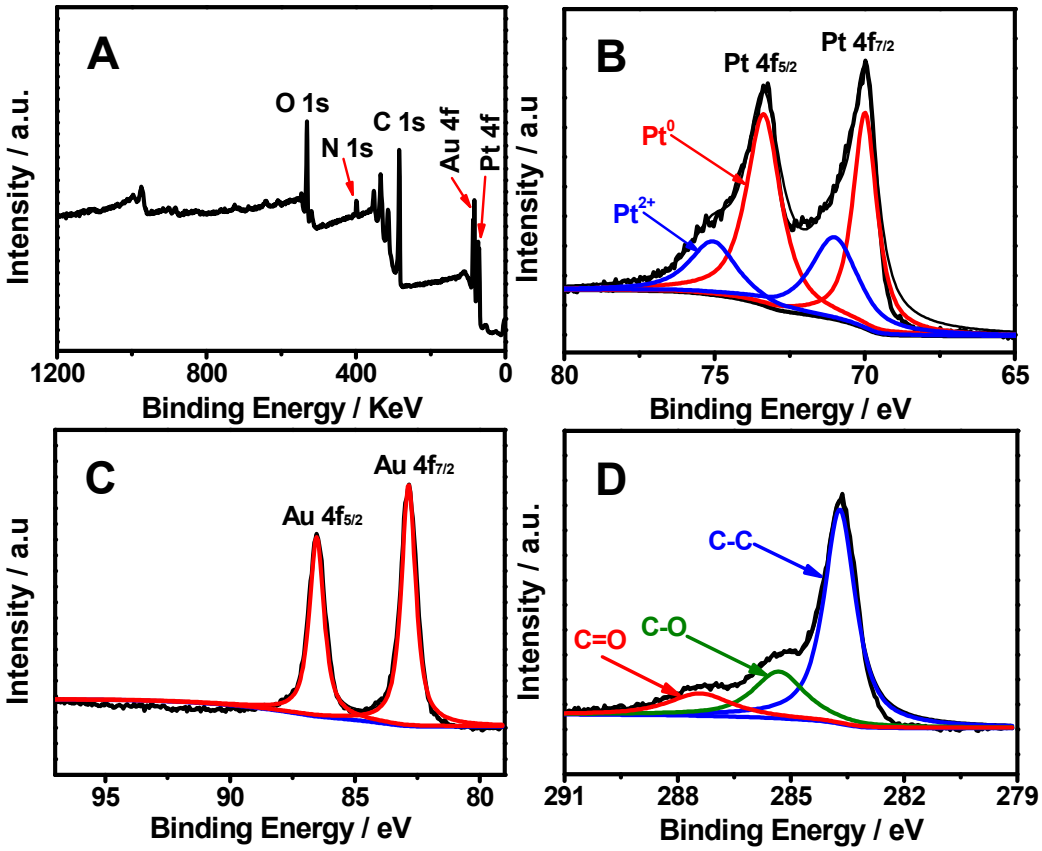

Fig. 6

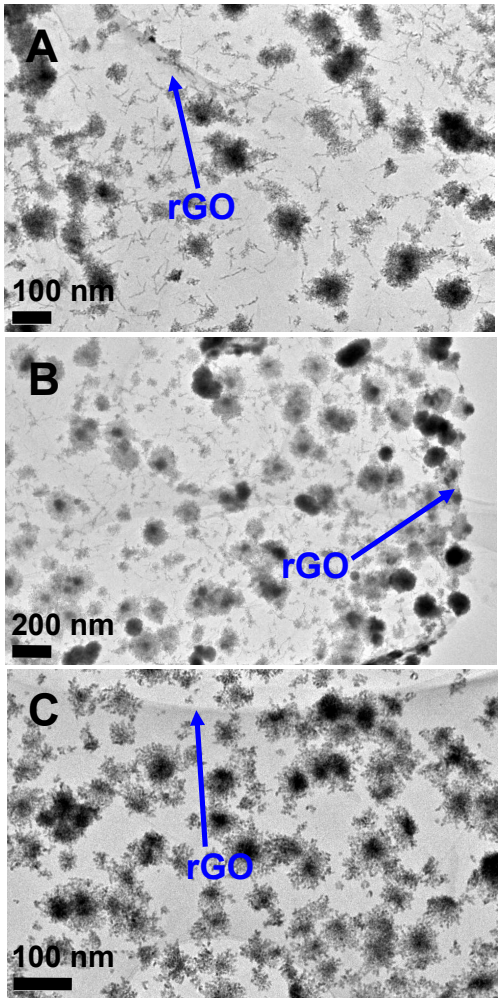

Fig. 7

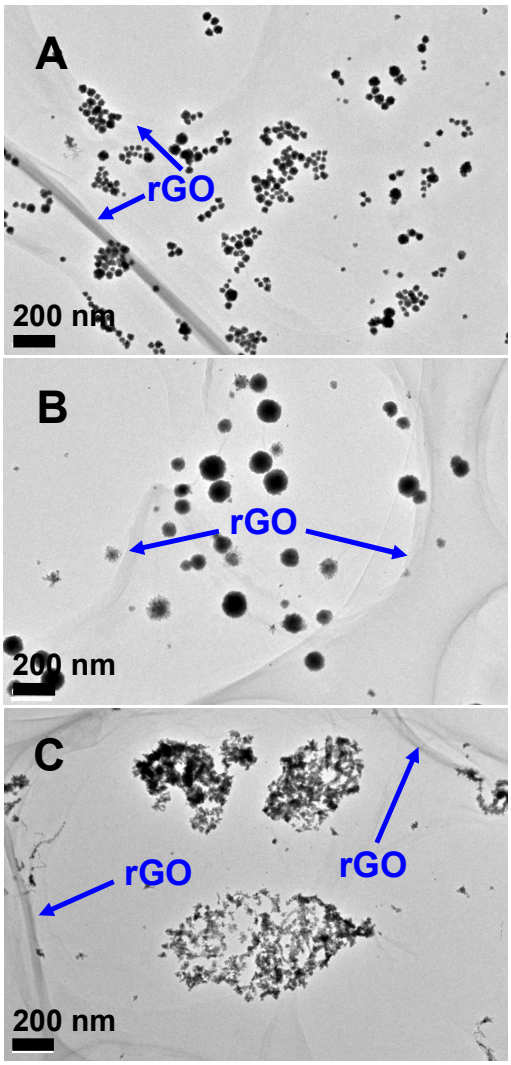

Fig. 8

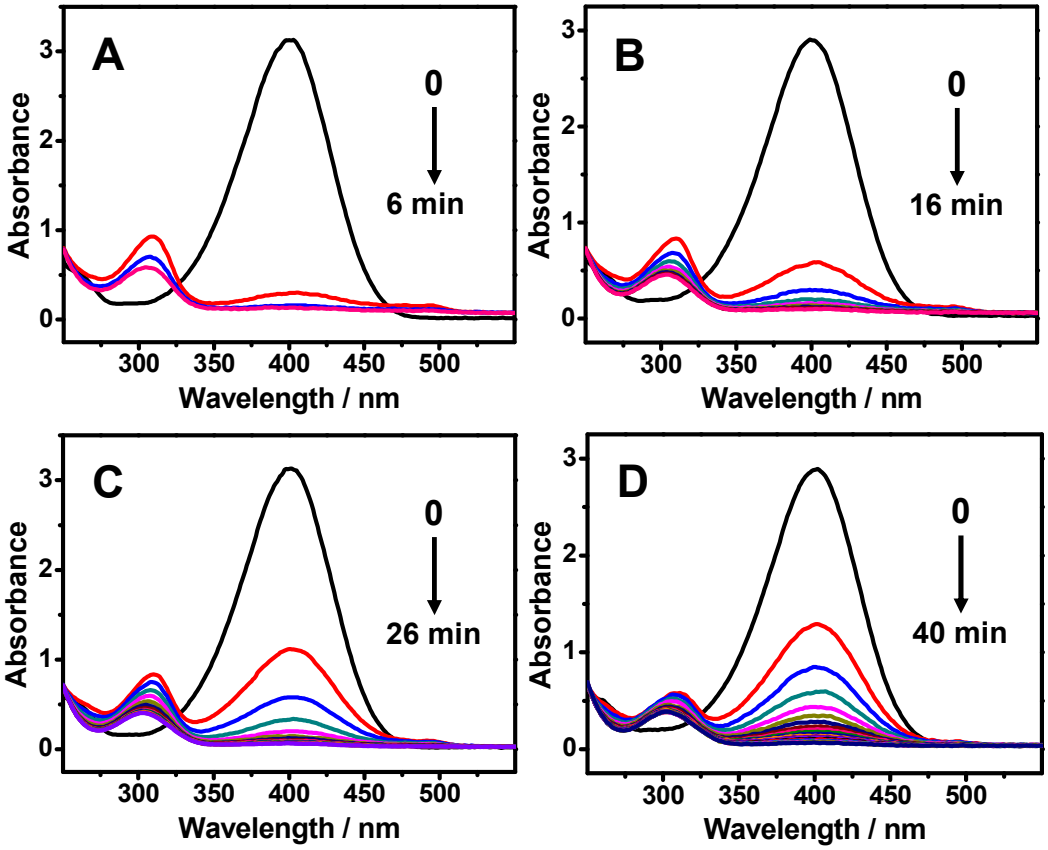

Fig. 9

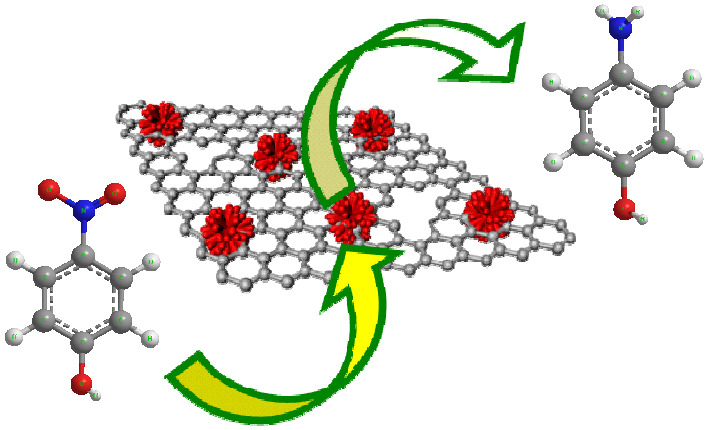

Fig. 10

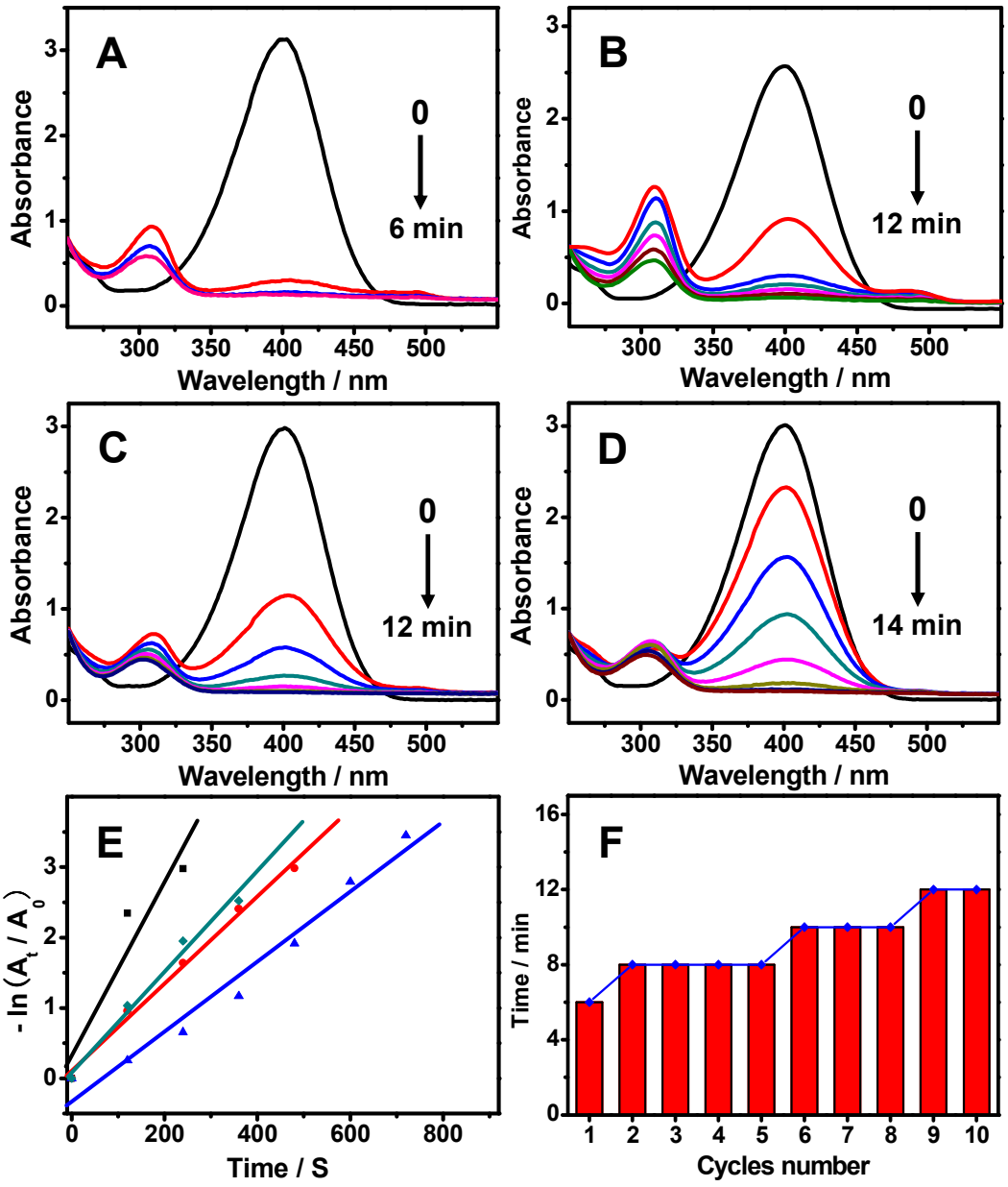

Graphical Abstract

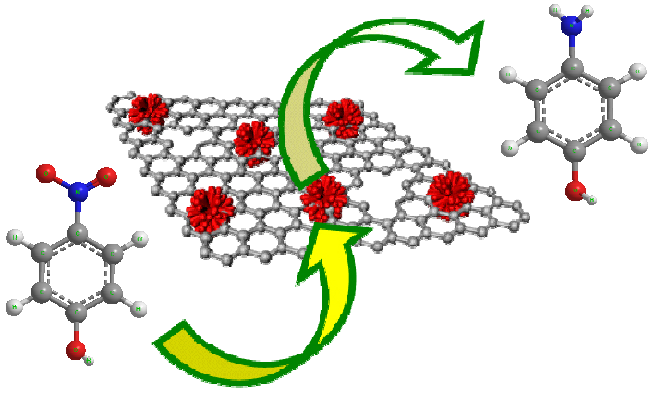

A simple and facile one-pot wet-chemical co-reduction method was developed for synthesis of porous PtAu-nanoflowers/rGO with the assistance of *p*-aminopyridine. No any seed, template, surfactant or polymer was involved. The as-prepared nanocomposites displayed excellent catalytic activity for 4-nitrophenol reduction.